electronics

MDPI

Article

# Dynamic Temperature Compensation of Pressure Sensors in Migratory Bird Biologging Applications

**Jinlu Xie [1,2], Zhitian Li [1] and Xudong Zou [1,*]**

[1] State Key Laboratory of Transducer Technology, Aerospace Information Research Institute, Chinese Academy of Sciences, Beijing 100190, China; xiejinlu17@mails.ucas.ac.cn (J.X.); ztli@mail.ie.ac.cn (Z.L.)
[2] School of Electronic, Electrical and Communication Engineering, University of Chinese Academy of Sciences, Beijing 100049, China
* Correspondence: xdzou@mail.ie.ac.cn

**Abstract:** This article proposes an improved dynamic quantum particle swarm optimization (DQPSO) algorithm to optimize a radial basis function (RBF) neural network for temperature compensation of pressure sensors used in tracking and monitoring wild migratory birds. The algorithm incorporates a temperature-pressure fitting model that includes temperature rate of change and gradient reference terms. It also includes a loss function that considers fitting accuracy and complexity, thereby improving the robustness of the sensor for complex temperature variations. The calibration experiments revealed that after implementation, the average absolute error of the pressure sensor output during dynamic temperature changes was reduced from 145.3 Pa to 20.2 Pa. This reduction represents an 86% improvement over the commercial polynomial compensation method, and the DQPSO approach significantly outperformed traditional feedforward network models. Finally, the algorithm was deployed and verified in an embedded environment for low-power, high-precision, real-time pressure compensation during the tracking and monitoring of wild migratory birds.

**Keywords:** biologging; pressure sensor; temperature compensation; radial basis function neural network; dynamic temperature change



**Citation:** Xie, J.; Li, Z.; Zou, X. Dynamic Temperature Compensation of Pressure Sensors in Migratory Bird Biologging Applications. *Electronics* **2023**, *12*, 4373. https://doi.org/10.3390/electronics12204373

Academic Editor: Nakkeeran Kaliyaperumal

Received: 8 October 2023
Revised: 17 October 2023
Accepted: 20 October 2023
Published: 22 October 2023



## 1. Introduction

Movement ecology is a cross-disciplinary academic field focused on the study of movement. Its aim is to enhance the comprehensive theory of biological movement in order to gain a better understanding of the mechanisms, patterns, causes, and impacts of all movement phenomena [1]. Moreover, ecologists strive to explore the impact of habitat change and climate change on the future by studying the causes and consequences of individual movement, understanding individual behavior and the spatial dynamics of groups at higher organizational levels. They also focus on the interactions between individuals and the environment [2].

Biologgers are a common type of sensor microsystem based on Lagrangian methods. They are typically composed of microcontrollers, microsensors, data storage units, data transmission units, and other combinations based on specific requirements. Using a biological recorder for non-proximity sampling not only reduces the impact of human activities on wildlife but also tracks and observes the movement status and physiological indicators of target individuals.

Migratory birds are birds that migrate periodically with the changing seasons. Among the existing 10,000 species of birds, more than 1800 are migratory birds. The number of individual birds migrating globally has reached billions or even tens of billions. This massive movement of bird populations is not only a specific manifestation of global climate change but also has a significant impact on the maintenance and stability of the global ecosystem structure and function [3]. Migration is a complex phenomenon that involves a series of physiological changes. It is characterized by predictable, continuous, and directional movements of animals, such as migratory birds, between different environments. This behavior allows organisms to maximize their adaptability to the environment by taking advantage of the productivity benefits offered by different seasons and locations [4]. Therefore, tracking and sampling the movement status and physiological indicators, known as "biologging", of migratory birds can help biologists understand the natural movement patterns of birds, and is of great significance for studying the survival status of migratory birds, carrying out ecological protection of migratory birds, and observing global ecosystem changes. Figure 1 shows our research object, the spotted goose, as well as some biologger studies applied to birds. Research [5] described an implantable instrument deployed in a project studying the high altitude Himalayan migrations of bar-headed geese, which can collect motion and ECG information for years. However, compared to implantable devices, wearable biological recorders (such as sensing tags [6]) have a smaller impact on the health of migratory birds.

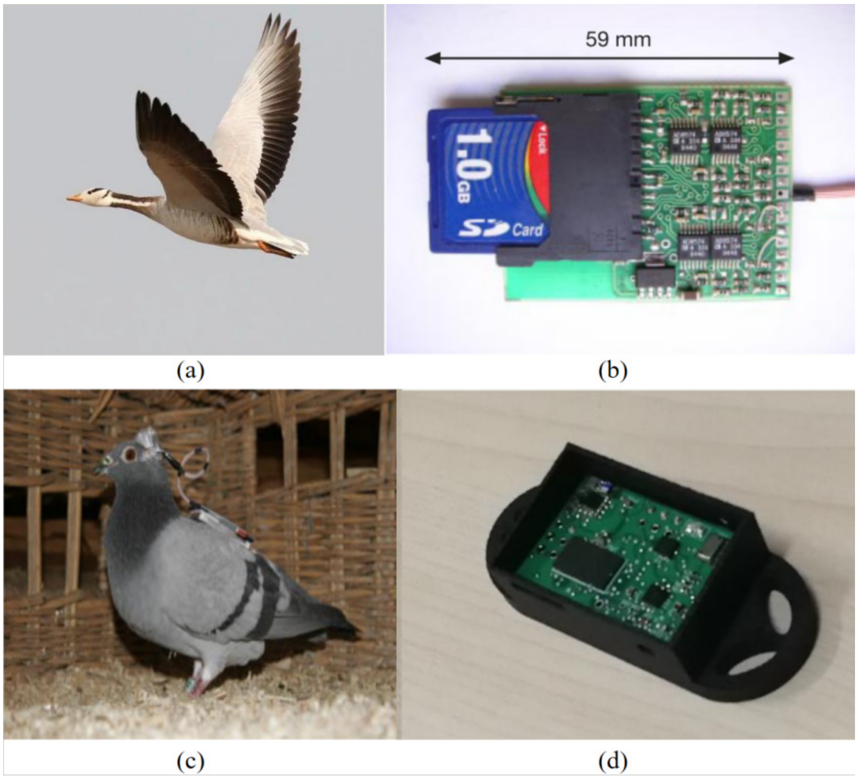


**Figure 1.** (**a**) Large migratory bird, the bar-headed goose, in flight. (**b**) Neurologger: collects pigeon EEG signals and GPS position information and records them on an SD card [7]. (**c**) Neurologger installed on the head and back of carrier pigeons. (**d**) Wearable biologger for birds collects information on heart rate, blood oxygen saturation, acceleration, magnetic field, air pressure, and temperature.

Barometric pressure is an important environmental parameter that is influenced by various factors, including temperature, geographical coordinates, altitude, and weather. As a result, it can be used to measure relevant environmental variables in the fields of meteorological monitoring, aerospace, and equipment manufacturing. In bird biological recording scenarios, barometric pressure can describe the environmental meteorological conditions and also indicate the flight altitude of birds when combined with positional information. This makes it an important factor in measuring 3D position information during bird migration. Large migratory birds can migrate up to tens of thousands of kilometers, flying up to roughly 3000–4000 m above sea level at speeds of up to 80 km/h. During migration, these birds navigate across plateaus and encounter highly dynamic and challenging high-altitude environments characterized by wide swings in temperature and pressure [8,9]. Therefore, a set of barometric pressure monitoring methods that can handle complex, temperature-varying environments is required to meet the field biological recording needs of large migratory birds. These methods should also be small, reliable, and easy to deploy in an embedded system. This is particularly important when considering the limited mass, volume, and power consumption of the biological recorders that can be carried by migratory birds.

In recent years, there has been rapid development in and widespread use of various types of micro-electromechanical systems (MEMS) barometric pressure sensors thanks to the advancement of MEMS technology. Based on their operating mechanisms, these sensors can be classified into different categories, such as capacitive, piezoresistive, resonant, and piezoelectric sensors [10]. Compared to capacitive barometric pressure sensors that exhibit low sensitivity and a nonlinear input-output relationship, resonant barometric pressure sensors that can be expensive, and piezoelectric barometric pressure sensors that have weak anti-jamming performance, piezoresistive barometric pressure sensors, designed and produced by utilizing the piezoresistive effect of semiconductor materials, offer several advantages. These sensors provide high sensitivity, good linearity, excellent stability, and low cost, and as a result are more suitable for barometric pressure monitoring in biological recording scenarios [11]. However, the detection performance of piezoresistive barometric pressure sensors is significantly influenced by temperature due to the thermal properties of semiconductor materials. Liu et al. showed that the error of the barometric pressure sensor becomes more pronounced as the temperature gets closer to the low-temperature condition [12]. Additionally, the error of the barometric pressure sensor in a low-pressure environment is influenced by temperature more than in a high-temperature environment. Therefore, it is necessary to calibrate the temperature compensation of barometric pressure sensors in biological recording scenarios to minimize the impact of complex dynamic environments with high and low temperatures on barometric pressure measurement accuracy.

Existing barometric pressure sensor temperature compensation methods can be divided into two categories: hardware compensation and software compensation. Due to the high cost, limited universality, and technical complexity, hardware compensation alone cannot fully meet the demands of engineering applications [13–15]. As a result, researchers and scholars worldwide are actively exploring different software compensation algorithms. Liu employed artificial neural networks to mitigate temperature drift in pressure sensors with promising outcomes [16]. Another approach described by Wang et al. involved the use of segmental fusion that combined linear fitting with a particle swarm-optimized radial basis function (RBF) neural network method [17]. This approach demonstrated improved results in terms of fitting error and computation time. Another study by Qiao explored the optimization of a BP (Back Propagation) neural network using an artificial fish school-frog hopping algorithm to fit barometric data, showing superiority over traditional genetic algorithms [18]. In the context of barometric altitude detection, Jia et al. proposed the use of wavelet functions to enhance the performance of the BP neural network, thereby reducing barometric nonlinear error [19].

Among the existing methods, the mainstream idea is to use intelligent algorithms to optimize RBF or BP neural networks. The RBF neural network has several advantages over other feedforward neural network models, such as its simple structure, fast training speed, and strong generalizability. Additionally, the RBF neural network radial basis function local response characteristics align well with the requirements of the barometric sensor for fitting local nonlinear errors caused by high and low temperatures. Unfortunately, the current compensation methods are designed for static states and do not address the issue of response hysteresis in complex temperature change environments, and their high algorithm complexity makes them unable to meet the requirements of low power consumption, fast response, and stable deployment in migratory bird biological recording scenarios.

To overcome current limitations in RBF neural network methods for migratory bird biological recording, we propose an improved air pressure compensation algorithm in this paper. The algorithm, based on the existing low-power bird wearable physiological information acquisition system [20], is designed to address the challenges posed by complex temperature-variable environments, such as low-pressure, low-temperature, and high-dynamic working conditions using the limited computational resources of embedded devices. The temperature-pressure fitting model can enhance the sensor's robustness in a dynamic temperature-variable environment, and the improved loss function can achieve a balance between model accuracy and complexity, ensuring real-time monitoring of the equipment's field environment.

The chapters of this paper are introduced as follows: In Section 2, the dynamic temperature change model and an improved dynamic quantum particle swarm optimization (DQPSO) algorithm are introduced. In Section 3, the new compensation algorithm is verified by the dynamic environment simulation experiment, data analysis, and embedded platform deployment. Section 4 is the conclusion of this paper.

## 2. Dynamic Quantum Particle Swarm Optimization Radial-Based Neural Network Algorithm

In this section, a local thermodynamic equivalent model of the sensing device is established, and an improved dynamic quantum particle swarm optimization (DQPSO) algorithm is proposed to optimize a radial basis function (RBF) neural network. The algorithm incorporates a temperature-pressure fitting model that includes terms for temperature rate of change and gradient reference, as well as a loss function that balances fitting accuracy and complexity.

### *2.1. Dynamic Temperature Change Model*

For modeling temperature-varying environments, which is common in the study of crystal oscillators and gyroscopes, two influences are generally considered: the temperature gradient and rate of change [21–23]. In temperature-changing environments, errors in piezoresistive pressure sensors are mainly caused by thermal zero drift, changes in thermal sensitivity, and thermal hysteresis effects [24].

Heat conduction is not uniform with rapid changes in ambient temperature due to the presence of a protective shell for the device and the varying thermal time constants between the barometric pressure sensor and the temperature sensor. This leads to a localized temperature gradient and hysteresis in relation to the ambient temperature, and the thermodynamic equivalent model is illustrated in Figure 2. The temperature sensors we used were usually MEMS Si band-gap temperature sensors with a digital processor integrated, and the pressure sensors were chosen due to their performance in sensitivity, linearity, stability, and cost. The change in barometric pressure can be considered instantaneous, but the hysteresis of temperature disrupts the coupling relationship between the local temperature of the sensor and the barometric pressure, introducing errors in the measurement of barometric pressure.

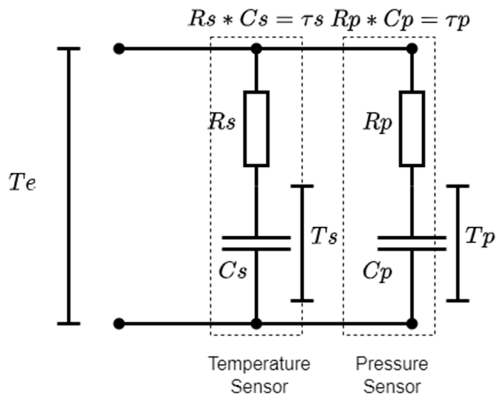


**Figure 2.** Local thermodynamic equivalent model of the sensing device comprised of a pressure sensor and a temperature sensor.

At time $t$, the temperature at the barometric pressure sensor and temperature sensor can be expressed, respectively, as

$$T_p(t) = T_e(t) \times (1 - \exp(-\Delta t/\tau_p)) + T_p(t - \Delta t) \times \exp(-\Delta t/\tau_p) \tag{1}$$

$$T_s(t) = T_e(t) \times (1 - \exp(-\Delta t/\tau_s)) + T_s(t - \Delta t) \times \exp(-\Delta t/\tau_s) \tag{2}$$

where $\tau_s$ and $\tau_p$ denote the thermal time constants of the temperature and barometric pressure sensors, respectively, and $\Delta t$ denotes a slight change in time ($\Delta t > 0$). Commonly, the ambient temperature, $T_e(t)$, is calculated based on the temperature sensor output temperature, $T_s(t)$, which is

$$T_e(t) = \frac{T_s(t) - T_s(t - \Delta t) \times \exp(-\Delta t/\tau_s)}{1 - \exp(-\Delta t/\tau_s)} \tag{3}$$

When the ambient temperature changes, the change in temperature at the temperature sensor and at the pressure sensor is not equal due to different thermal time constants and thermal gradient distributions, as shown in Figure 1. Moreover, the temperature variation pattern at the same location in the device is not always the same, due to the randomness of the heating mode and local heat conduction process of the equipment. Therefore, it is not sufficient to only consider the temperature rate of change to accurately model the temperature field in its entirety in the traditional model. It is also necessary to include a description of the temperature gradient between the barometric pressure sensor and the environment, and this can be achieved by introducing additional temperature measurement points with fixed relative positions. This leads to our dynamic temperature change model. In practice, temperature sensors and barometric pressure sensors are often placed on the same circuit board, and we assume that all temperature measurement points would be on the same geometric plane as the barometric pressure sensor. The distribution of temperature gradients measured at multiple locations can be considered a map of the temperature distribution between the barometric pressure sensor and the ambient temperature, and the introduction of multiple temperature point measurements can capture the distribution of temperature gradients as a factor that influences barometric pressure compensation. In general, the dynamic temperature change model incorporates a greater number of temperature measurement points and takes into account the distribution of local temperature gradients in the device. This provides more environmental information for pressure temperature compensation compared to the traditional model. In our model, the estimation error of pressure is influenced not only by the resolution, sensitivity, and stability of the sensor itself, but also by the dynamic distribution of heat in time and space. In fact, this applies to any sensor that is affected by temperature.

### *2.2. Quantum Particle Swarm Optimization Algorithm*

Particle swarm is a classical algorithm for intelligent optimization proposed by Kenney and Eberhart in 1995 [25]. The algorithm was developed based on the flight behavior in bird flocks and incorporates the concepts of individual evolution and knowledge transfer through the continuous cooperation and competition of many particles. Each particle continuously updates its position based on the individual optimal value and the group optimal value to realize the search for the global optimal solution in a complex space. Compared to other swarm intelligent optimization algorithms, the particle swarm algorithm is simple to operate, fast to train, and avoids complex genetic mutation and other processes, and since the algorithm was proposed, researchers have made various detailed improvements to the speed and position update process [25,26]. In this paper, we optimize the structural and computational parameters of the radial-based neural network using the quantum particle swarm algorithm [27–29]. The algorithm establishes a particle swarm model based on quantum and potential wells, which introduces more randomness to the model, improves global convergence performance, reduces the number of control parameters, and enhances optimization searching ability.

There are N initialized particles, and the execution process of the algorithm is as follows:

**Step 1:** Randomly initialize the positions of all particles, $X_i(0),\ i = 1, 2, \cdots, N$, and calculate the initial global optimal position, $G(0)$, and the initial average optimal position, $C(0)$, of all particles according to the objective fitness function

$$C(n) = \frac{1}{N}\sum_{i=1}^{N} P_i(n) \tag{4}$$

where $P_i(n)$ denotes the optimal position of the $i$th particle of the nth theory evolution.

**Step 2:** Randomly update the position of each particle according to

$$X_i(n+1) = \varphi(n) \cdot P_i(n) + [1 - \varphi(n)] \cdot G(n) \pm \alpha \cdot |C(n) - X_i(n)| \cdot \ln[1/u_i(n)] \tag{5}$$

where the summed proportional weights are chosen randomly for the individual and global optimal solutions so that $\varphi(n) \sim U(0,1)$ (uniform distribution between 0 and 1). In the last part of Equation (4), $\alpha$ is the innovation parameter. It has been proven by theory and random simulation experiments that in the algorithm with the evolution Equation (4), the necessary and sufficient condition for the convergence of a single particle is $\alpha < 1.782$ [27]. In addition, $u_i(n) \sim U(0,1)$ can generate a randomized positional term based on potential wells, so the sign before alpha in Equation (4) is chosen at random with a 50% probability of a positive sign or a negative sign.

**Step 3:** According to the target fitness function, update the current fitness values of all particles as well as the individual optimal position, the global optimal position, and the global average optimal position.

**Step 4:** Check if the iteration end condition has been met, and if so, end the optimization search process; otherwise, repeat steps 2 and 3.

### *2.3. Temperature-Pressure Fitting Model with Loss Function*

Piezoresistive barometric sensors produce nonlinear errors in both high- and low-temperature regions, and temperature compensation essentially involves solving a nonlinear function fitting problem. Radial basis neural networks map low-dimensional data inputs to higher dimensions by means of radial basis functions, thus transforming a problem that is not linearly differentiable in low-dimensional space into a linearly differentiable problem in high-dimensional space [30]. It has been proven that on a compact set, the radial basis neural network can approximate any nonlinear function with arbitrary accuracy [31]. Compared with other feed-forward neural network models, the radial basis neural network has the advantages of simple structure, fast training speed, and strong generalizability. Furthermore, the radial basis function has the characteristic of local response, which is beneficial for the high- and low-temperature nonlinear error fitting requirements of barometric sensors.

Synthesizing the theoretical analysis outlined in the previous two sections, this paper proposes an innovative four-input and two-output radial basis neural network model. The model incorporates the temperature rate of change and temperature gradient as inputs and improves the iterative loss function by synthesizing the constraints on the model's fitting accuracy and complexity, as shown in Figure 3. The input variables include raw data for air pressure, raw data for multi-temperature points, the temperature rate of change, and the temperature gradient. The output variables are the ambient temperature and ambient air pressure.

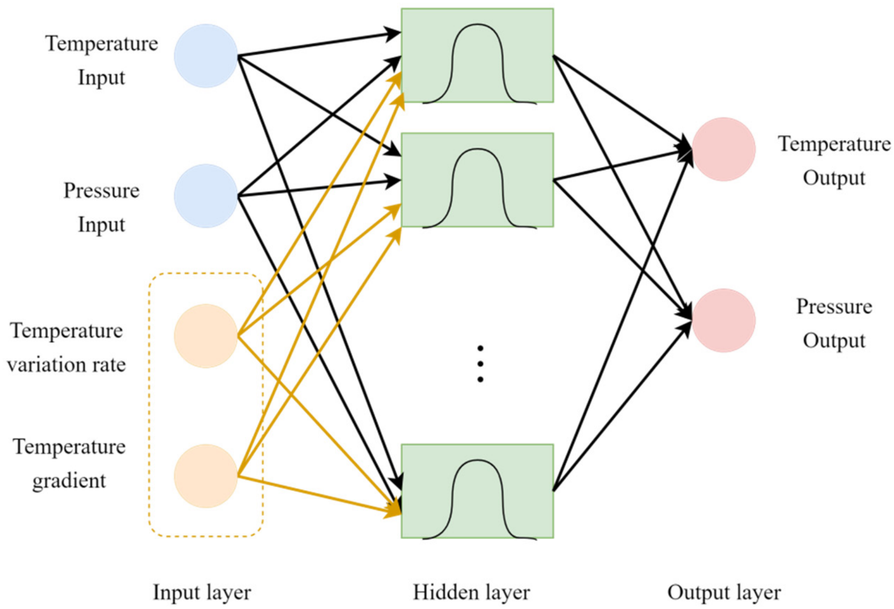


**Figure 3.** Radial basis neural network model with temperature variation rate and temperature gradient input nodes.

The radial basis neural network is highly influenced by the choice of the centers of the hidden layer basis function, which are generally selected using the K-means algorithm. However, in the case of barometric sensor temperature and pressure calibration points, they are uniformly spaced dot matrix inputs. The position of the clustering center can be adjusted by manipulating the density distribution of the input data, which helps optimize the performance of local nonlinear fitting. Therefore, the distribution of the basis function centers can be adjusted to be more uniform and more densely distributed in high- and low-temperature nonlinear regions. In this paper, the optimization parameters for the model are selected as the number of nodes in the hidden layer and the variance of the Gaussian radial basis function. The iteration end condition is set to reach the maximum number of iterations or the loss function no longer decreases.

The quantum particle swarm algorithm is utilized to optimize these two variables globally on the fitness function set, ultimately obtaining the temperature-pressure fitting model with optimal accuracy and complexity. In order to distinguish it from the method of optimizing radial basis function neural networks using traditional particle swarm optimization algorithms (QPSO-RBF), the method proposed in this paper is named Dynamic QPSO-RBF (DQPSO-RBF). The model training would need to be completed in a lab environment prior to sensor field deployment.

If the true value of ambient barometric pressure for the $i$th data set is $P_{i,e}$ and the model fit barometric pressure value is $P_{i,o}$, the average mean square error given by:

$$\text{MSE} = \frac{1}{N}\sum_{i=1}^{N}(P_{i,o} - P_{i,e})^2 \tag{6}$$

and the average absolute error given by:

$$\text{MAE} = \frac{1}{N}\sum_{i=1}^{N}|P_{i,o} - P_{i,e}| \tag{7}$$

can be used to assess the model's accuracy. By analyzing the output error results, the fitness function, or loss function, is constructed to maintain a comparable order of magnitude between the model error MSE and the number of nodes P in the hidden layer of the network. The loss function is given by:

$$\text{loss} = \log(\text{MSE}) + \mu(\text{P}) \tag{8}$$

where $\mu(\text{P})$ is the penalty term for the number of nodes in the hidden layer, which is $\mu(p) = \beta \cdot p (0 < \beta < 0.5)$ in this paper.

In summary, the steps for constructing the temperature and pressure fitting model of the particle swarm algorithm-optimized radial basis neural network designed in this paper are shown in Figure 4.

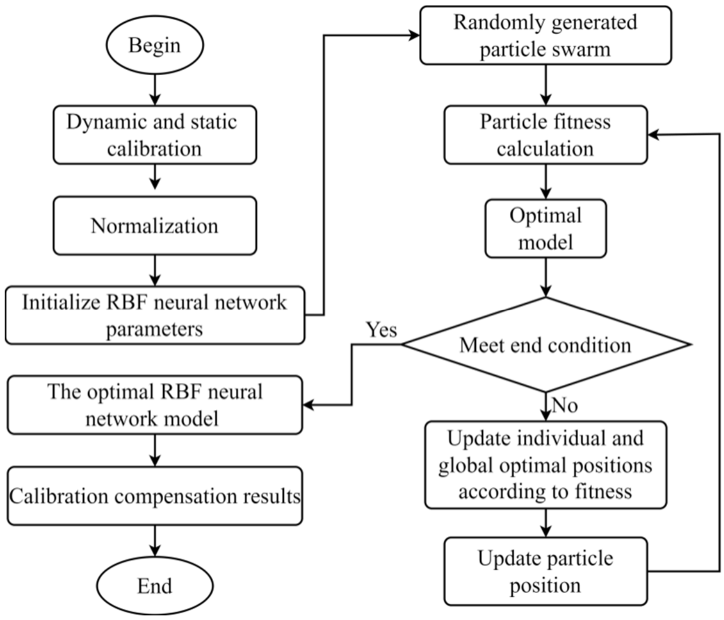


**Figure 4.** Algorithm modeling steps.

## 3. Experimental Verification of Calibration

In this section, the RBF net was trained as the steps introduced in Section 2 and the algorithm's compensation effect was verified by simulating the flight environments and motion states of migratory birds. Compared to other traditional methods, the DQPSO-RBF algorithm has demonstrated significant advantages and has been validated for embedded deployment.

### *3.1. Data Acquisition*

The goal of the data acquisition process is to establish the relationship between temperature and pressure under static conditions. The experiment involved using a temperature box (ESPEC SH-241) to regulate the ambient temperature and a barometric pressure controller (Druck PACE 5000) to regulate the ambient barometric pressure. The sensing device used in our biologger was placed inside a copper container, which was mechanically sealed and used to isolate internal and external air pressure, and positioned within the temperature box, as depicted in Figure 5. In the experiment, the MS5837 barometric pressure sensor from TE Connectivity was selected, and the temperature calibration range was set to −20 °C to 65 °C with the barometric pressure calibration range set to 700 hPa to 1100 hPa. The barometric pressure was sampled every 5 kPa, and the barometric pressure controller at each point was left to stabilize for 1 min. The temperature was sampled every 5 °C, and the temperature box at each point was left to stabilize for 60 min. This process yielded 162 static calibration points for temperature and pressure.

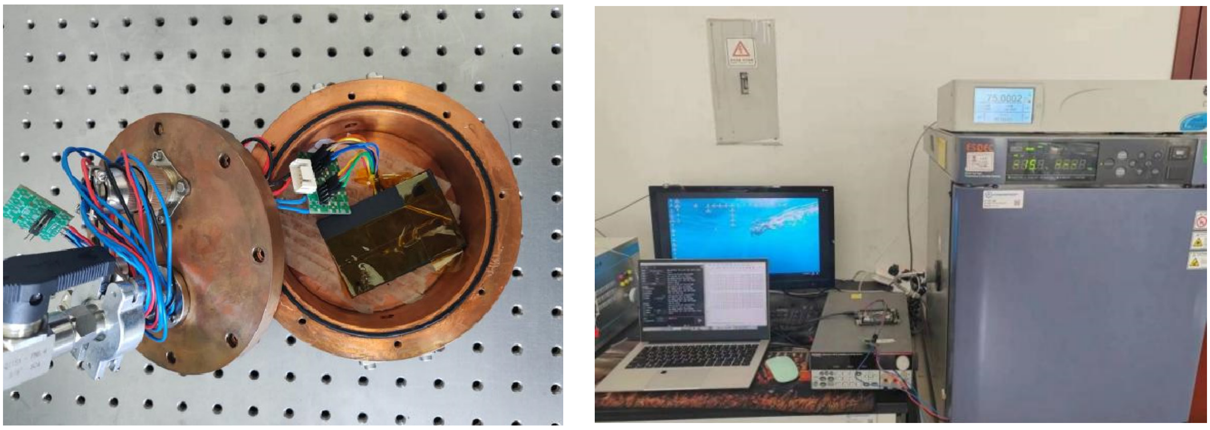

(**a**) (**b**)

**Figure 5.** Experimental environment for data acquisition, including the copper container (**a**) and the temperature box (ESPEC SH-241) (**b**).

### *3.2. Dynamic Environment*

The dynamic environment simulation experiment aimed to simulate the high-altitude flight environment of migratory birds and verify the algorithm's compensation performance in complex temperature-varying environments. In the experiment, sensing devices were placed in a TV-10-70-W temperature chamber to expose the sensors to high and low temperatures. The internal ambient air pressure was controlled by the barometric pressure controller to maintain a constant level, while the ambient temperature was controlled by the temperature controller to facilitate high- and low-temperature cyclic changes. The experimental setup is illustrated in Figure 6.

(**a**) (**b**)

**Figure 6.** Dynamic environment simulation experiment, including the TV-10-70-W temperature chamber (**a**) and sensing device inside (**b**).

In the dynamic environment simulation experiment, the temperature inside the chamber varied within the range of −20 °C to 65 °C. The air pressure value was kept constant, and two calibration points of 90 kPa and 70 kPa were set up to simulate the actual environment of migratory birds flying at high altitudes. These calibration points corresponded to the dynamic temperature-varying environments at heights of approximately 1 km and 3 km, respectively. In the experiment, the control temperature was rapidly cooled from 25 °C to −20 °C, left to stabilize for 30 min, and then rapidly warmed up to 65 °C. The temperature was left to stabilize for another 30 min at 65 °C before being cooled back down to 25 °C, completing a cycle. The temperature ramp rate during the experiment was set to 1 °C/min. Dynamic experiments were conducted with a sampling frequency of 1 Hz to continuously acquire raw data output of sensor temperature and pressure while the real temperature and pressure changes in the environment were recorded simultaneously. Figure 7 shows the temperature and pressure changes during the dynamic experiment at 90 kPa and 70 kPa under the temperature change cycle process.

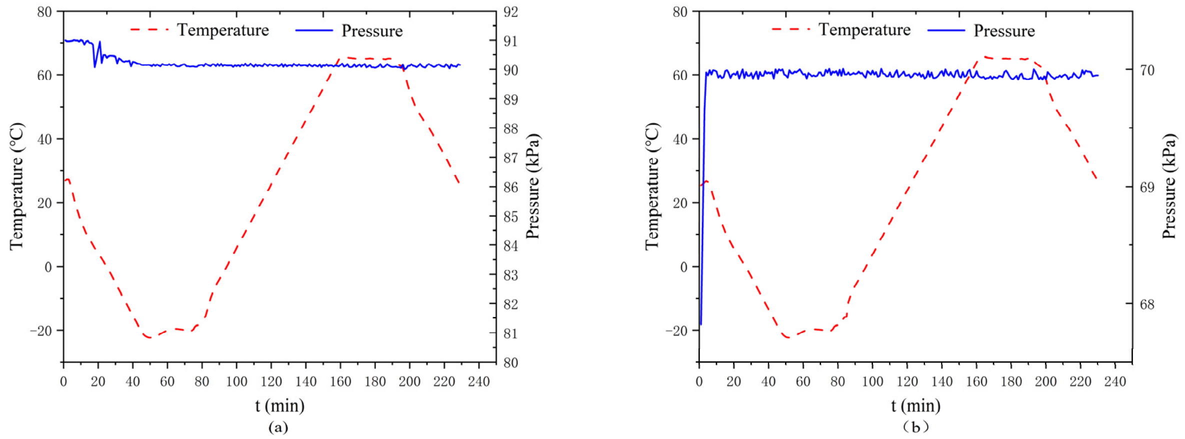


**Figure 7.** Ambient temperature and pressure change in the dynamic environment simulation experiments with ambient air pressures of 90 kPa (**a**) and 70 kPa (**b**).

### 3.3. Data Analysis

After performing the above-mentioned experiments, the collected data were used to train the neural network model. All the original data were normalized to [0,1] and input into the radial basis neural network model with a randomly selected 10% of the data reserved as the test set. The model setting parameters are shown in Table 1.

**Table 1.** Model setting parameters.

| Model Parameter | Numerical Value |
|---|---|
| Number of particle swarms | 20–50 |
| Max number of iteration rounds | 10–30 |
| Number of hidden layer neuron p | 3–30 |
| Radial basis function variance σ | 0.01–10 |
| Innovation parameter α | 0.8 |
| penalty factor β | 0–0.5 |

Accurate numbers of hidden layer neuron and radial basis function variance were determined by algorithm during training, and we mainly made manual adjustments on a number of particle swarms and penalty factor Increasing the penalty factor would suppress the expansion of the RBF network, thereby reducing the number of neurons in the final hidden layer, but it can also lead to an increase in average error, and vice versa. Therefore, it is necessary to adjust the parameters appropriately to strike a balance between model accuracy and complexity. If computing resources are sufficient, more particles can be added to the swarm. By adjusting the model's setting parameters, the optimal metrics for the radial-based neural network model were selected, as shown in Table 2 with the number of hidden layer nodes set to 14.

**Table 2.** Parameters of model results.

| Resulting Parameters | Numerical Value |
|---|---|
| Number of hidden layer nodes | 14 |
| Radial basis function variance | 1.039120 |
| Loss function | −2.338029 |
| Average mean square error MSE | $6.485676 \times 10^{-10}$ |

In the dynamic environment, the initial training model was enhanced by introducing temperature gradient and temperature rate of change terms that improved the model's adaptability to complex temperature changes. The portion of the dynamic calibration data that shows significant temperature changes was sampled at a rate of 10%, and the model was trained together with the static calibration data. The results of the absolute errors recorded over time for different compensation methods in the dynamic environment are shown in Figure 8.

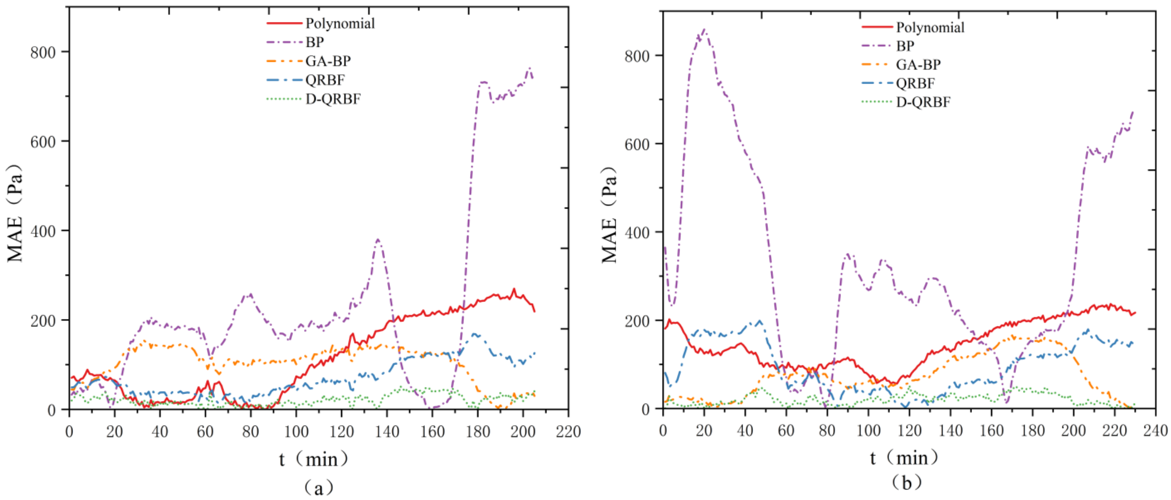


**Figure 8.** Mean absolute error of ambient air pressure in the dynamic environment simulation experiments with ambient air pressures of 90 kPa (**a**) and 70 kPa (**b**).

Table 3 demonstrates the compensation results of the algorithm proposed in this paper compared to the polynomial compensation, the traditional RBF neural network, the traditional RBF neural network, and the BP neural network optimized by genetic algorithm (GA-BP) under 90 kPa and 70 kPa environmental experimental scenarios. The polynomial compensation method originates from the pressure sensor manufacturer, including temperature and pressure compensation exceeding third order, and the specific calculation parameters were calibrated during the manufacturing process, while other methods rely on calibration data obtained from our experiments. Polynomial compensation showed a greater error during the heating stage than during the cooling stage. The BP neural network provided better MAE in the temperature static stage, but it amplified the error locally during the temperature change stage. Although the error gradually decreased during the temperature stabilization stage, it still resulted in an overall increase in average error throughout the process. Although the BP neural network method has a slight advantage in terms of computational complexity compared to compensation methods from manufacturers, the average errors are much larger. GA-BP is another commonly used sensor compensation algorithm [32]. After a relatively complex iterative process of genetic variation, GA-BP showed limited error in the whole dynamic processes; however, it still exhibited sensitivity to the heating process.

**Table 3.** Algorithm compensation MAE for different dynamic environments.

| Experimental Scenario | Polynomial Compensation | BP ($N$ = 14) | GA-BP ($N$ = 14) | QPSO-RBF ($N$ = 14) | DQPSO-RBF ($N$ = 14) |
|---|---|---|---|---|---|
| Dynamic environment (90 kPa) | 114.3 | 234.8 | 103.3 | 71.2 | 21.1 |
| Dynamic environment (70 kPa) | 145.3 | 333.9 | 73.6 | 94.5 | 20.2 |

On the other hand, the improved QPSO-RBF algorithm presented in this paper demonstrated greater adaptability in dynamic environments without causing a significant increase in error. The best performance was achieved by the DQPSO-RBF algorithm, which incorporated a dynamic temperature-pressure model to compensate for errors in dynamic environments. The DQPSO-RBF algorithm demonstrated the best performance, especially after implementing the dynamic temperature and pressure model. This improvement led to further enhancement in compensating for errors throughout the temperature-variation cycle. The algorithm maintained relatively stable performance, with the absolute error consistently below 50 Pa. Additionally, the average absolute error was reduced to 21.1 Pa and 20.2 Pa for ambient air pressures of 90 kPa and 70 kPa, respectively.

To evaluate the effect of the model and algorithm presented in this paper in reducing the complexity of the RBF neural network model, the compensation error of the proposed algorithm was compared to that of the RBF neural network model with varying numbers of nodes. This comparison was based on the data collected from the calibration process, as depicted in Figure 9.

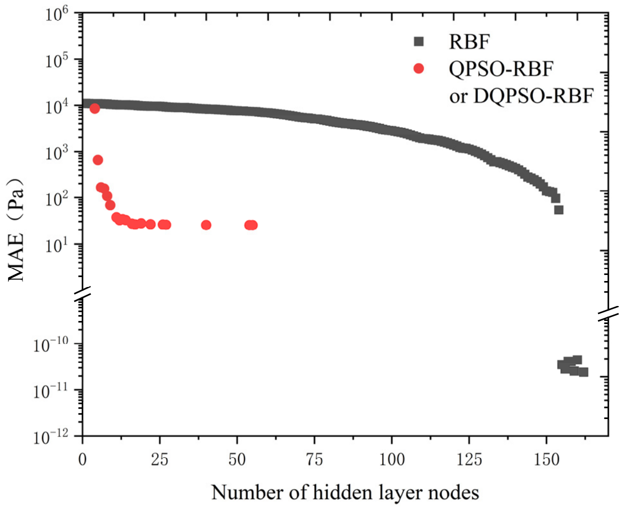


**Figure 9.** Mean absolute error of ambient air pressure for different RBF neural network models versus the number of hidden layer nodes.

Theoretically, if the number of nodes in the hidden layer of the radial-based neural network is sufficiently large, it can approximate any nonlinear function with arbitrary accuracy. However, reducing the number of nodes can lead to rapid amplification of the error when using the traditional model training method. Furthermore, the computation requirements of a radial-based neural network are proportional to the number of nodes in the hidden layer, and as the number of nodes in the hidden layer increases, the more unfavorable the model becomes for low-power, real-time computation in an embedded environment. The results show that the algorithm presented in this paper can provide a significant advantage in compensating for small node count networks. We found the optimal number of nodes to be approximately 14 in our implementation of the DQPSO-RBF algorithm.

In order to minimize the impact of biologgers on the flight of migratory birds, the internationally accepted standard is to restrict the weight of recorders to 3% of the bird's body weight. In our research project, the weight limit for the device is strictly set at 35 g in total. This weight includes sensors, data storage units, microprocessors, batteries, casings, and other components. Therefore, in the case of limited system computing resources, the computational cost of any algorithm must be strictly controlled. To validate the practical deployment capability of the DQPSO-RBF algorithm on embedded platforms, we deployed and verified the algorithm using the STMicroelectronics STM32L0 very low-power embedded platform with a Cortex M0+ core. Figure 10 shows several of the embedded platforms we used for testing and deployment. In outdoor scenarios, biological recorders do not continuously collect all sensor data. Instead, they collect data at regular intervals or when rapid environmental changes are detected. Although the compensation algorithm for the pressure sensor is not the only code running on the platform, the sampling programs do not all work simultaneously. Therefore, we only run this program here and utilize Systick of Arm core for precise timing. The algorithm was set to a quantization accuracy of 6 bits and converted floating-point computation to fixed-point computation, and the final algorithm model storage occupied less than 512 bytes. The platform we used has 8 KBytes of RAM and 64 Kbytes of Flash, so it is enough for model deployment and calculation. We ran the program 100 times consecutively, collecting data from the pressure sensor and applying our compensation algorithm. Afterward, we calculated an average time of 25 ms for sampling and compensation, which fully meets the sampling requirements for real-time tracking of wild migratory birds. We believe that the calculation time is determined by the processor performance, main clock frequency, and peripheral communication frequency. In the experiment, we set the main clock frequency of STM32L0 to 32 MHz, and the I2C bus speed for communication with sensors to 400 Kbit/s. If we disregard the need for low power consumption and field deployment, the algorithm's computational performance can be enhanced even further.

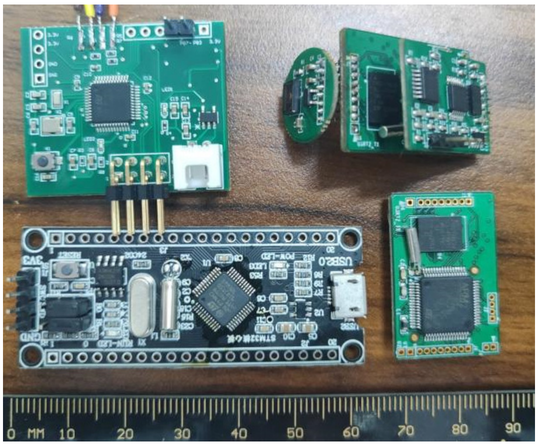


**Figure 10.** Several STM32L0 embedded platforms with sensors integrated.

The reason why we are unable to conduct simulated flight experiments on migratory birds is that our research subject, the spotted goose, is a protected animal of the highest class in China. Therefore, conducting experiments on migratory birds requires a longer review cycle, and the results of the flight simulation test of the biologgers will be published in future academic reports.

## 4. Conclusions

In this paper, we proposed an innovative temperature compensation algorithm to enhance the performance of the dynamic quantum particle swarm (DQPSO) optimized radial basis neural network for piezoresistive barometric pressure sensors. The algorithm addressed the issues of nonlinear errors in high- and low-temperature environments encountered by piezoresistive barometric pressure sensors in biological recording scenarios of wild migratory birds as well as the hysteresis errors in scenarios involving dynamic temperature changes. The temperature-pressure fitting model introduced the terms of temperature change rate and temperature gradient reference, where these terms were used to enhance the algorithm's adaptability in dynamic temperature-varying environments. The loss function included a penalty term and was used to regulate the complexity of the model while maintaining model accuracy. The compensation accuracy, robustness, and model complexity of the algorithm were verified through dynamic simulation experiments in a migratory bird flight environment. Under dynamic environmental conditions, the

DQPSO-RBF algorithm reduced the average absolute error of the barometric pressure sensor from 145.3 Pa to 20.2 Pa after compensation. This represents an 86% decrease compared to the polynomial compensation method from its producer, and the DQPSO-RBF algorithm significantly outperformed the traditional feed-forward neural network model. The algorithm was also verified in an embedded environment using the STMicroelectronics STM32L0 platform where the average time for a single compensation calculation was roughly 25 ms. This technology can assist biologists in accurately monitoring environmental pressure and flight altitude during the high-altitude migration of migratory birds. This allows scientists to gain a better understanding of the migration patterns of birds in extreme environments.

**Author Contributions:** Conceptualization, J.X. and Z.L.; methodology, J.X.; software, J.X.; validation, J.X. and Z.L.; resources, X.Z.; data curation, J.X.; writing—original draft preparation, J.X.; writing—review and editing, J.X., Z.L., and X.Z.; visualization, J.X.; supervision, J.X. and X.Z.; project administration, Z.L. and X.Z.; funding acquisition, X.Z. All authors have read and agreed to the published version of the manuscript.

**Funding:** This research was funded by the Research Instrument and Equipment Development Project of the Chinese Academy of Sciences (Grant NO. YJKYYQ20210023).

**Data Availability Statement:** Not applicable.

**Conflicts of Interest:** The authors declare no conflict of interest.

## References

1. Nathan, R. An emerging movement ecology paradigm. *Proc. Natl. Acad. Sci. USA* **2008**, *105*, 19050–19051. [CrossRef] [PubMed]
2. Schick, R.S.; Loarie, S.R.; Colchero, F.; Best, B.D.; Boustany, A.; Conde, D.A.; Halpin, P.N.; Joppa, L.N.; McClellan, C.M.; Clark, J.S. Understanding movement data and movement processes: Current and emerging directions. *Ecol. Lett.* **2008**, *11*, 1338–1350. [CrossRef] [PubMed]
3. Green, A.J.; Elmberg, J. Ecosystem services provided by waterbirds. *Biol. Rev.* **2014**, *89*, 105–122. [CrossRef] [PubMed]
4. Lennox, R.J.; Chapman, J.M.; Souliere, C.M.; Tudorache, C.; Wikelski, M.; Metcalfe, J.D.; Cooke, S.J. Conservation physiology of animal migration. *Conserv. Physiol.* **2016**, *4*, cov072. [CrossRef] [PubMed]
5. Spivey, R.J.; Bishop, C.M. An implantable instrument for studying the long-term flight biology of migratory birds. *Rev. Sci. Instrum.* **2014**, *85*, 1. [CrossRef]
6. Toledo, S.; Mendel, S.; Levi, A.; Vortman, Y.; Ullmann, W.; Scherer, L.-R.; Pufelski, J.; van Maarseveen, F.; Denissen, B.; Bijleveld, A.; et al. Vildehaye: A Family of Versatile, Widely-Applicable, and Field-Proven Lightweight Wildlife Tracking and Sensing Tags. In Proceedings of the 2022 21st ACM/IEEE International Conference on Information Processing in Sensor Networks (IPSN), Milan, Italy, 4–6 May 2022; pp. 1–14. [CrossRef]
7. Vyssotski, A.L.; Serkov, A.N.; Itskov, P.M.; Dell'Omo, G.; Latanov, A.V.; Wolfer, D.P.; Lipp, H.-P. Miniature Neurologgers for Flying Pigeons: Multichannel EEG and Action and Field Potentials in Combination with GPS Recording. *J. Neurophysiol.* **2006**, *95*, 2. [CrossRef]
8. Altshuler, D.; Dudley, R. The physiology and biomechanics of avian flight at high altitude. In *Integrative and Comparative Biology*; Oxford University Press Inc.: New York, NY, USA, 2006; Volume 46, pp. 62–71. [CrossRef]
9. Gill, R.; Tibbitts, T.; Douglas, D.; Handel, C.; Mulcahy, D.; Gottschalck, J.; Warnock, N.; McCaffery, B.; Battley, P.; Piersma, T. Extreme endurance flights by landbirds crossing the Pacific Ocean: Ecological corridor rather than barrier? *Proc. R. Soc. B Biol. Sci.* **2009**, *276*, 447–458. [CrossRef]
10. Peng, L. Design of a New MEMS Piezoresistive Pressure Sensor. Master's Thesis, University of Electronic Science and Technology, Chengdu, China, 2021. Available online: https://kns.cnki.net/KCMS/detail/detail.aspx?dbname=CMFD202201&filename=1021747547.nh (accessed on 10 September 2023).
11. Zaiqi, W.; Jinlong, J.; Yihui, L.; Junjian, L. Research on Temperature Characteristics of a Piezoresistive Pressure Sensor. *Metrol. Test. Technol.* **2022**, *6*, 37–40. [CrossRef]
12. Hongtao, L.; Xiaoyong, P.; Yandong, W. Analysis of Effect of Ambient Temperature on Measurement Error of Air Pressure Sensors. *Autom. Instrum.* **2022**, *6*, 60–64. [CrossRef]
13. Honglin, H.; Jiahao, X.; Zhanhong, Z.; Dongming, H.; Ji, L. Research on Interpolation Compensation Method for Temperature Error of Piezo-resistive Pressure Sensor. *J. Electron. Meas. Instrum.* **2021**, *12*, 1–7. [CrossRef]
14. Pereira, R.D.S.; Cima, C.A. Thermal Compensation Method for Piezoresistive Pressure Transducer. *IEEE Trans. Instrum. Meas.* **2021**, *70*, 1–7. [CrossRef]
15. Liu, Z.; Du, L.; Zhao, Z.; Liu, J.; Wu, P.; Fang, Z. A chip-level oven-controlled system used to improve accuracy of silicon piezoresistive pressure sensor. *Measurement* **2019**, *143*, 1–10. [CrossRef]

16. He, L. Research on Temperature Compensation Method for Silicon Piezoresistive Pressure Sensors Based on Artificial Neural Networks. Master's Thesis, Huaibei Normal University, Huaibei, China, 2020. Available online: https://kns.cnki.net/KCMS/detail/detail.aspx?dbname=CMFD202002&filename=1020066189.nh (accessed on 10 September 2023).
17. Hui, W.; Guochao, Z.; Xin, J.; Yuning, S. Temperature compensation method for piezoresistive sensor based on Piecewice fusion. *J. Sens. Technol.* **2018**, *4*, 562–566.
18. Weide, Q. Temperature Compensation for Pressure Sensors Based on BP Neural Network Model. *J. Huaiyin Norm. Univ. (Nat. Sci. Ed.)* **2019**, *4*, 322–327. [CrossRef]
19. Kebin, J.; Yanming, W.; Jiachun, Y.; Pengyu, L. Nonlinear correction ofpressure sensors based on neural network. *J. Beijing Univ. Technol.* **2021**, *1*, 40–49.
20. Yifan, Z.; Mengyao, L.; Xudong, Z. Design of low power consumptionbio-datalogger for birds. *Foreign Electron. Meas. Technol.* **2019**, *9*, 60–65. [CrossRef]
21. Zhihao, C. The Calibration of Testing System and Data Model Analysisfor The Dynamic Frequency Temperature Characteristics of Crystal Oscillator. Master's Thesis, Shandong University of Science and Technology, Qingdao, China, 2020. Available online: https://kns.cnki.net/KCMS/detail/detail.aspx?dbname=CMFD202101&filename=1020103442.nh (accessed on 10 September 2023).
22. Xiaoli, H.; Yuanbo, T. Zero bias compensation of multiple temperature points of prism laser gyro. *Electron. Technol.* **2017**, *6*, 138–141. [CrossRef]
23. Xianfei, P.; Jie, Y.; Meiping, W. RLG bias compensation method in complex temperature variation environments. *Chin. J. Inert. Technol. Rep.* **2011**, *2*, 234–238. [CrossRef]
24. Qinglin, T.; Hongliang, C.; Hongmin, C.; Liang, L.; Wenji, Y. A full-temperature-range temperature compensation method for piezoresistive pressure sensor. *China Test.* **2021**, *1*, 49–53.
25. Kennedy, J.; Eberhart, R. Particle swarm optimization. In Proceedings of the ICNN'95-International Conference on Neural Networks, Perth, WA, Australia, 27 November–1 December 1995; Purdue University System. pp. 1942–1948. [CrossRef]
26. Krohling, R. Gaussian swarm: A novel particle optimization algorithm. In Proceedings of the 2004 IEEE Conference on Cybernetics and Intelligent Systems, Singapore, 1–3 December 2004; Volumes 1 and 2, pp. 372–376.
27. Jun, S. Paticle Swarm Optimization with Particles Having Quantum Behavior. Ph.D. Thesis, Jiangnan University, Wuxi, China, 2010. Available online: https://kns.cnki.net/kcms2/article/abstract?v=PhqKDHt8vRCmheqjKPIazP-OKlbEsSfnu5FhI9sofVeQVJlf-BBdGyXWxfoYcxAYLFy_q71JcL49O2JhRkB532-2b1I6nNuURMDbglVecpSpxTb4r8_PEqfwlTIcbO0a&uniplatform=NZKPT&language=CHS (accessed on 10 September 2023).
28. Rongcheng, S. Research on Fractional Order PID Magnetic Levitation Bearing Controller Based on Quantum Particle Swarm Optimization Algorithm. Master's Thesis, Wuhan University of Technology, Wuhan, China, 2021. Available online: https://kns.cnki.net/KCMS/detail/detail.aspx?dbname=CMFD202301&filename=1022722231.nh (accessed on 10 September 2023).
29. Wu, X.; Deng, F.; Chen, Z. RFID 3D-LANDMARC Localization Algorithm Based on Quantum Particle Swarm Optimization. *Electronics* **2018**, *2*, 19. [CrossRef]
30. Defeng, Z. *MATLAB R2020a Neural Network Typical Case Analysis*; Electronic Industry Press: Beijing, China, 2021.
31. Chunyu, Q.; Yongzhuang, H.; Ziqi, G.; Fangxu, H.; Xiuping, W. New Sliding Mode Control Based on Tracking Differentiator and RBF Neural Network. *Electronics* **2022**, *11*, 3135. [CrossRef]
32. Yang, H.; Yang, Y.; Hou, Y.; Liu, Y.; Liu, P.; Wang, L.; Ma, Y. Investigation of the Temperature Compensation of Piezoelectric Weigh-In-Motion Sensors Using a Machine Learning Approach. *Sensors* **2022**, *22*, 2396. [CrossRef] [PubMed]